A Complete Microwave Characterization of GaAs HEMTs under Optical Illumination

Alina Caddemi[1], Giovanni Crupi[1], Enza Fazio[2], Salvatore Patanè[2], and Giuseppe Salvo[1]

Abstract – **The present paper is devoted at presenting the main results of an extensive experimental investigation of the microwave transistor behaviour under optical illumination. The tested devices are on-wafer HEMTs based on AlGaAs/GaAs heterostructure. The light sensitivity of these transistors is investigated in terms of DC, scattering and noise parameters. The analysis is carried out by observing how the device behaviour changes under CW infrared and visible laser illumination. It is found that the light exposure affects significantly the device behaviour. In particular, the main changes consist of an increase of the drain current, the transconductance, the forward transmission coefficient, and the minimum noise figure. The optical effects have shown to be more pronounced at shorter wavelength. The observed effects of the laser illumination can be ascribed to the threshold voltage shift arising from the internal photovoltaic effect.**

Keywords – **Gallium arsenide, light exposure, microwave transistor, noise parameters, scattering parameters, threshold voltage shift.**

I. INTRODUCTION

The gallium arsenide (GaAs) high-electron-mobility transistor (HEMT) has demonstrated to be a mature and well-established technology, which is an excellent candidate for high-frequency low-noise applications. In light of that, many studies have been dedicated to investigating the noise performance of GaAs HEMTs [1]-[10]. It should be highlighted that the physical properties of III-V compound semiconductors, as well as the typical layer structure, make this type of transistor extremely attractive for integrated communication systems, where the microwave signal is optically controlled. Therefore, the investigation of the HEMT behaviour under optical illumination is of great interest. Different experimental results have been achieved, since the optical effects can significantly depend on the particular case of study (e.g., device physics and structure, bias condition, frequency range, optical power, and radiation wavelength). The attention has been mainly devoted to the study of the DC characteristics and scattering (S-) parameters [11]-[20], while only a limited amount of results have been published with regard to the light exposure effects on the noise (N-) parameters [21], [22].

[1]Alina Caddemi, Giovanni Crupi, and Giuseppe Salvo are with the Dipartimento di Ingegneria Civile, Informatica, Edile, Ambientale e Matematica Applicata, University of Messina, Contrada di Dio, 98166 Messina, Italy, E-mail: acaddemi@unime.it; crupig@unime.it; gpp.salvo@gmail.com.

[2]Enza Fazio and Salvatore Patanè are with the Dipartimento di Fisica e di Scienze della Terra, University of Messina, Viale F. Stagno D'Alcontres 31, 98166 Messina, Italy, E-mail: enfazio@unime.it; patanes@unime.it.

The present paper is aimed at reporting on our recent research activity focused on a complete microwave characterization of GaAs HEMTs under optical illumination [23], [24]. The light sensitivity of the tested microwave devices is investigated in terms of DC, S- and N-parameters under CW infrared and visible laser illumination. Significant optical effects are observed. It is worth noting that the optical effects appear to be more pronounced at shorter wavelength. The achieved optical effects can be ascribed to the threshold voltage shift arising from the internal photovoltaic effect. The term “internal” refers to the fact that it has been not necessary to insert an external gate bias resistor to enhance the optical effects.

This article is structured into five sections. Section II is devoted at describing the studied devices and the experimental set-up. The tested devices are three AlGaAs/GaAs HEMTs with a gate width of 100 μm, 200 μm, and 300 μm. Their multifinger layout is based on paralleling two gate fingers. As well known, the multifinger layout allows reducing the gate resistance, which may have a critical impact on microwave characteristics, such as the noise performance. This is because more fingers in parallel leads to a wider path, not only for the drain current but also for the gate current, which implies a reduction of the gate resistance. The experimental set-up is electronically configured to switch by means of a switch driver between the noise calibration/measurement chain and the S-parameter measurement chain without removing any part or connection. The frequency range of the S- and N-parameter measurements is, respectively, limited to 26.5 GHz and 18 GHz. The noise parameters are determined with the source-pull procedure, which consists of measuring the noise figure for different source impedances synthesized by the source tuner.

Section III is aimed at analysing the effects of the light exposure on the DC characteristics. The main consequence of light exposure is a significant increase of the drain current and transconductance. With the aim to quantify the size of the optical effects, the associate threshold voltage shift is calculated.

Subsequently, the investigation is focused on the S- and N-parameters in Sections IV and V, respectively. Both S- and N-parameters are significantly affected by the light exposure. In particular, the magnitude of the forward transmission coefficient and the minimum noise figure resulted to be increased under optical illumination. Furthermore, to highlight the impact of the light exposure on the noise behaviour, the noise paraboloid, which represents the noise figure as a function of the source reflection coefficient, is reported for different operating frequencies with and without illumination.

Finally, the conclusive remarks of this experimental investigation are given in Section VI.

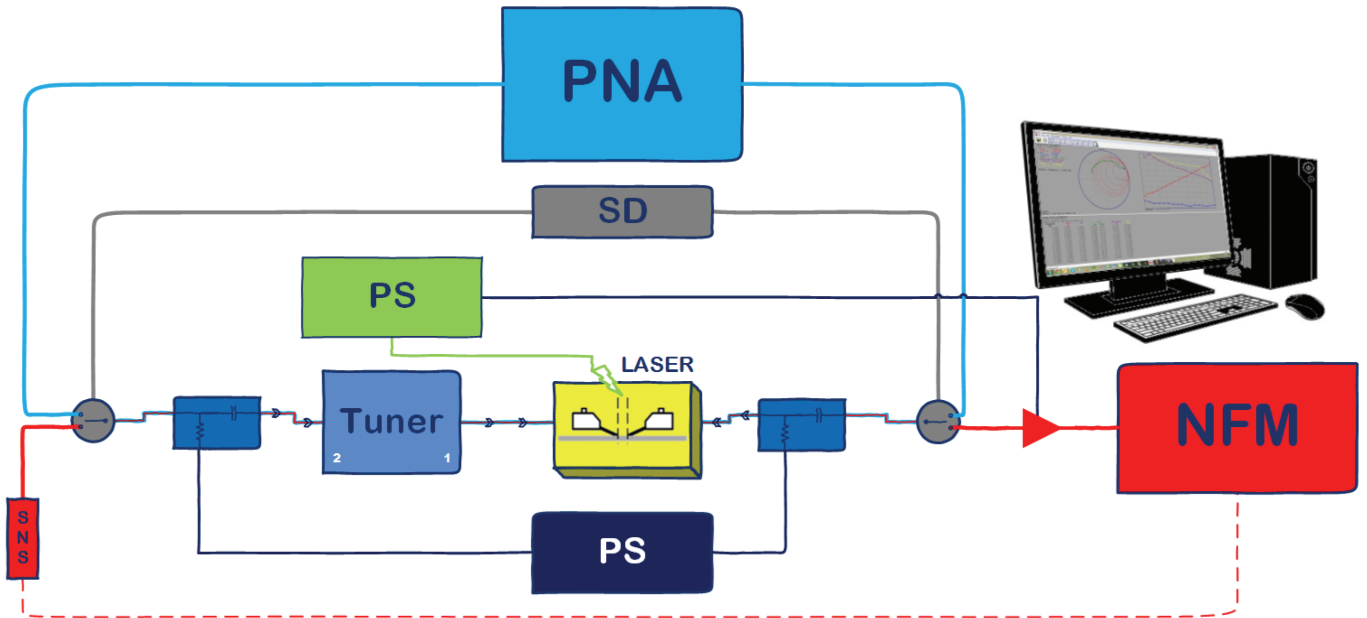

Fig. 1. Schematic diagram of the measurement set-up

II. Description of the Tested Devices and the Measurement Set-up

The studied microwave transistors are three HEMTs based on AlGaAs/GaAs heterostructure. These devices have a gate length of 0.25 μm and a gate width of 100 μm, 200 μm, and 300 μm. Their interdigitated layout consists of two fingers in parallel. The multi-finger layout allows improving the microwave characteristics, especially in terms of noise performance. The complete device series was originally diced from the wafer and glued onto a brass carrier.

The configuration of the experimental set-up is illustrated with a schematic diagram in Fig. 1. To contact the tested devices, a Cascade Microtech M150 on wafer station equipped with GSG (ground-signal-ground) probes has been used. An incident power density of about 0.3 $\mu W/\mu m^2$ has been used for the laser light stationary on one spot covering the entire area of the transistor. Such a value has been selected after several measurements by increasing the optical power to reach a level suitable to obtain noticeable effects on the microwave parameters of the transistor under test. Three different laser wavelengths have been chosen: 960 nm, 808 nm, and 650 nm.

A switch driver (SD) is used to switch between the noise calibration/measurement chain and the S-parameter measurement chain without removing any part or connection. In particular, the device input is connected to a tuner (Maury MT-983BU01, 2 ÷ 26.5 GHz), which is in turn connected via an electromechanical SPDT (single-pole-double-throw) switch to either the input port of the vector network analyzer (Agilent E8364A PNA, 0.045 ÷ 50 GHz) and the smart noise source (Agilent N4002A SNS, 10 MHz ÷ 26.5 GHz). The device output is connected via another SPDT switch to either the output port of the PNA and the input of the low noise receiver that includes a low noise amplifier (LNA) and the noise figure analyzer (Agilent N8975A NFA, 10 MHz ÷ 26.5 GHz). The power supplies (PS) are used for the laser, LNA, and to set the bias condition for the tested devices.

The S-parameter frequency range is limited to 26.5 GHz by the tuner and the switch/connectors, while the upper frequency of the N-parameters is limited to 18 GHz by the response band of the low-noise amplifier used in the receiver chain. The paths for S- and N- parameter measurements have been, respectively, represented with blue and red lines in the schematic diagram illustrated in Fig. 1.

The N-parameters are determined using the ATS Maury software according to a standard Y-factor source-pull procedure that allows driving automatically the calibration steps (i.e., in situ tuner calibration and noise receiver calibration) and the data processing/display.

The source-pull procedure consists of extracting the noise figure F (or noise figure NF when expressed in dB) for different source impedances synthesized by the source tuner at ON/OFF source noise levels. This procedure is based on expressing F as a function of the source reflection coefficient Γ_s by using the four N-parameters (i.e., minimum noise factor F_{min}, magnitude and phase of the optimum source reflection coefficient Γ_{opt}, and the noise resistance R_n) [2], [25]-[29]:

$$F = F_{min} + 4\frac{R_n}{Z_0}\frac{|\Gamma_s - \Gamma_{opt}|^2}{|1+\Gamma_{opt}|^2\left(1-|\Gamma_s|^2\right)} \quad (1)$$

where the reference impedance Z_0 is usually 50 Ω, F_{min} is the minimum value of F occurring when Γ_s equals Γ_{opt}, and R_n represents how fast F increases as Γ_s moves away from its optimum.

III. DC Characteristics under Optical Illumination

Fig. 2 shows the comparison between dark and illuminated DC characteristics of the HEMT with a gate width of 100 µm. In particular, the following plots have been reported: I_{DS} versus V_{DS}, I_{DS} versus V_{GS}, and g_m versus V_{GS}. The radiation wavelength has been set to at 650 nm. As can be noticed, the light exposure leads to a significant increase of I_{DS} and g_m. This result should be ascribed to the threshold voltage shift, due to the internal photovoltaic effect. As a matter of fact, it has been observed a clear shift of the I_{DS} – V_{GS} and the g_m – V_{GS} curves towards more negative values of V_{GS}.

In agreement with previous studies [16]-[20], the physical origin of the observed ΔV_{TH} can be attributed to the excess photo-generated holes drifting toward the source electrode region and then leading to a decrease of the potential barrier for the electrons in the channel. In light of that, the effect of the optical illumination can be seen as superimposing a forward bias to the gate that shifts the threshold voltage by a quantity ΔV_{TH}.

As reported in [16]-[18], the threshold voltage shift associated to the internal photovoltaic effect can be quantified as the slope of the straight line interpolating ΔI_{DS} as a function of g_m, where ΔI_{DS} consists of the current increase due to the light exposure. Fig. 3 shows how ΔV_{TH} has been determined for the device with a gate width of 100 µm under an optical illumination of 650 nm. In the present case, to estimate ΔV_{TH}, the values of I_{DS} and g_m have been taken at moderately low V_{DS} (i.e., V_{DS} = 2 V), before the onset of the observed rapid increase of I_{DS} at higher V_{DS}. It has been obtained a ΔV_{TH} equal to 165 mV.

Three different laser wavelengths have been used for the device with a gate width of 300 µm: 960 nm, 808 nm, and 650 nm [24]. The obtained values of ΔV_{TH} are reported in Table I. It has been found that the light sensitivity increases at shorter wavelength. Hence, the analysis has been focused on the optical illumination at 650 nm. At room temperature the 808 nm light allows band-to-band transitions in the GaAs layer (1.4 eV), whereas the red light at 650 nm is able to excite the transitions in both GaAs and AlGaAs (typically around 1.8 eV) layers enhancing the optical effects. The exposure to the 960 nm beam should not cause any effect because the photon energy is lower than the GaAs bandgap. Nevertheless, a slight DC current increase was observed. We argued that broadening mechanisms occur in the GaAs layer. Hence, the observed phenomena may be ascribed to several classical process in semiconductors such as band-tailing and free-carrier absorption mechanisms, as well as to a photon-assisted tunnelling process occurring in presence of a strong electric field. This is the case for the electric field built up inside the GaAs quantum well 2-DEG upon biasing the device (Franz-Keldysh effect) [30].

Furthermore, the values of ΔV_{TH} have been calculated for the three scaled devices under the optical illumination at 650 nm [23]. As can be seen from Table II, the light sensitivity increases by reducing the gate width of the tested device. In light of that, the attention has been focused on the device with a gate width of 100 µm.

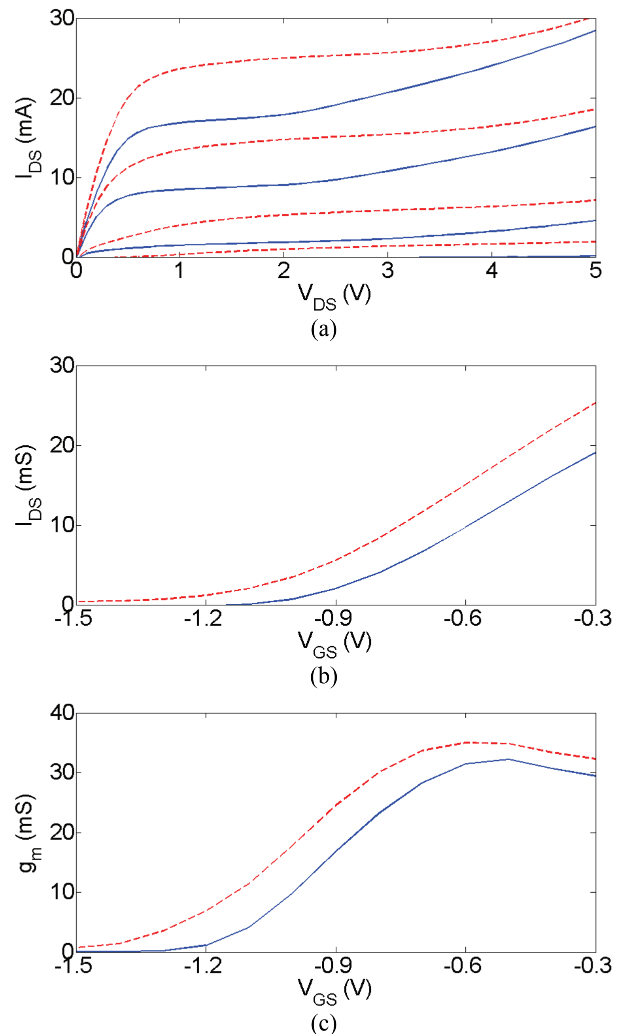

Fig. 2. DC characteristics without light (blue continuous lines) and under optical illumination at 650 nm (red dashed lines) for a 100-µm HEMT: (a) I_{DS} versus V_{DS} with V_{GS} varied from -1.2 V to -0.3 V in steps of 0.3 V, (b) I_{DS} versus V_{GS} at V_{DS} = 2.5 V, and (c) g_m versus V_{GS} at V_{DS} = 2.5 V

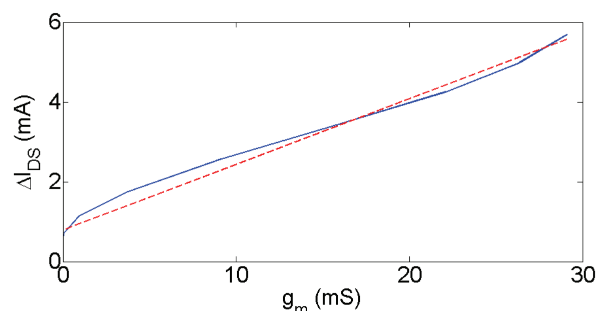

Fig. 3. Experimental data (blue continuous line) and associated interpolating lines (red dashed line) representing ΔI_{DS} versus g_m for a 100-µm HEMT at V_{DS} = 2 V. The values of ΔI_{DS} are obtained from the increase of the drain current under optical illumination at 650 nm

TABLE I
THRESHOLD VOLTAGE SHIFT FOR A HEMT WITH A GATE WIDTH OF 300 MM UNDER THREE DIFFERENT OPTICAL ILLUMINATIONS

Wavelength (nm)	960	808	650
ΔV_{TH} (mV)	34	54	77

TABLE II
THRESHOLD VOLTAGE SHIFT FOR THREE GAAS HEMTS WITH DIFFERENT GATE WIDTH UNDER OPTICAL ILLUMINATION AT 650 NM

Gate Width (μm)	100	200	300
ΔV_{TH} (mV)	165	111	77

IV. SCATTERING PARAMETERS UNDER OPTICAL ILLUMINATION

To perform the S-parameter measurements, the experimental set-up is electronically configured through the switch driver to connect the device to the input and the output ports of the PNA (see blue path in Fig. 1).

Since the optical effects on the DC characteristics have resulted to be more pronounced for the smaller device and at shorter wavelength, the investigation for S- and N-parameters is restricted to the device with a gate width of 100 mm and under an optical illumination at 650 nm.

Fig. 4 shows the comparison of the S-parameters with and without illumination at the bias condition point corresponding to the maximum g_m: V_{GS} = -0.6 V and V_{DS} = 2.5 V. As can be clearly seen, the S-parameters are significantly affected by the light exposure. It is worth noting that the main change is given by an increase of the magnitude of $|S_{21}|$, as highlighted in Fig. 5. This results should be ascribed to the observed increase of g_m in Fig. 2(c). To corroborate it, Fig. 6 shows that the light exposure leads to higher values of the low-frequency Re(Y_{21}), since at low frequencies Y_{21} tends to be a purely real quantity representing the RF extrinsic transconductance.

To investigate the bias dependence of the light sensitivity for the S-parameters, the analysis in Figs. 7-9 is focused on an extremely different bias condition: V_{GS} = -1.275 V and V_{DS} = 0 V. The measurements without illumination show that the S-parameters exhibit the typical behaviour for a HEMT at the pinch-off. On the other hand, due to the shift of V_{TH}, the measurements under optical illuminations show that S_{22} does not start from the open circuit condition and S_{21} is not equal to S_{12}.

V. NOISE PARAMETERS UNDER OPTICAL ILLUMINATION

To perform the N-parameter measurements, the experimental set-up is electronically configured through the switch driver to connect the SNS to the tuner and the device output to the noise receiver (see red path in Fig. 1).

Likewise the case of the S-parameters, the optical illumination leads to significant changes also in the behaviour of the N-parameters, as illustrated in Fig. 10.

It should be underlined that the irradiation leads to a remarkable increase of NF_{min} over the full frequency range. Such a result may appear to be in contrast with the achieved increase of g_m, $|Y_{21}|$, and $|S_{21}|$, which should imply a reduction in NF_{min}. However, the observed degradation of NF_{min} should be ascribed to the photo-generated charge accumulation leading to the onset of high diffusion noise processes in the channel [21], which plays a more dominant role than the increase of the device gain.

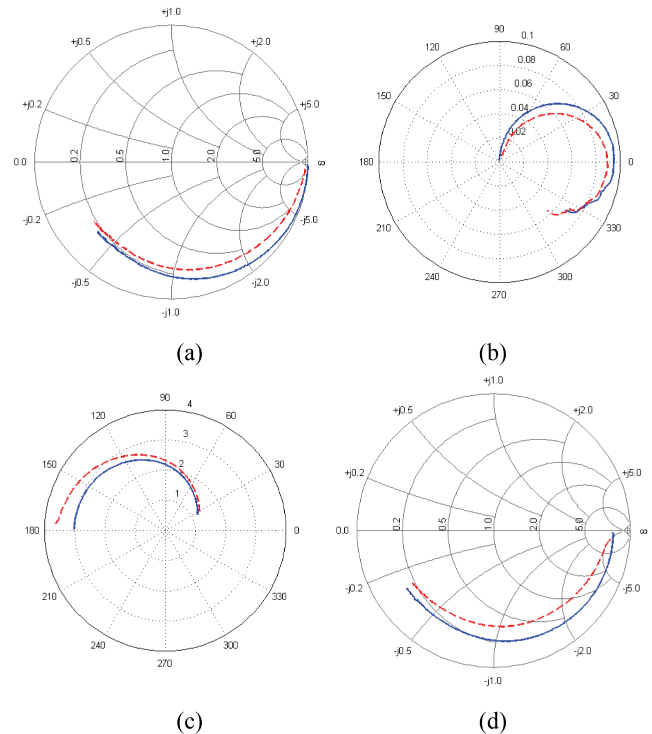

Fig. 4. S-parameters without light (blue continuous lines) and under optical illumination at 650 nm (red dashed line) for a 100-μm HEMT at V_{GS} = -0.6 V and V_{DS} = 2.5 V: (a) S_{11}, (b) S_{12}, (c) S_{21}, (d) S_{22}. The frequency ranges goes from 0.1 to 26.5 GHz

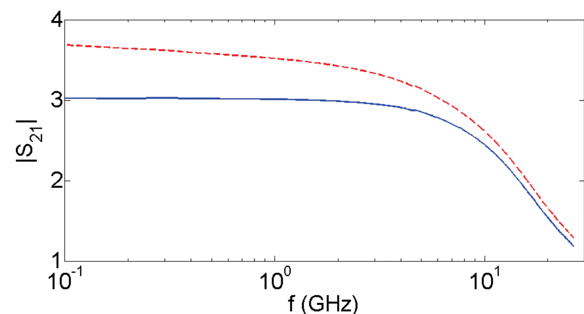

Fig. 5. Magnitude of S_{21} versus frequency without light (blue continuous line) and under optical illumination at 650 nm (red dashed line) for a 100-μm HEMT at V_{GS} = -0.6 V and V_{DS} = 2.5 V. The frequency ranges goes from 0.1 to 26.5 GHz

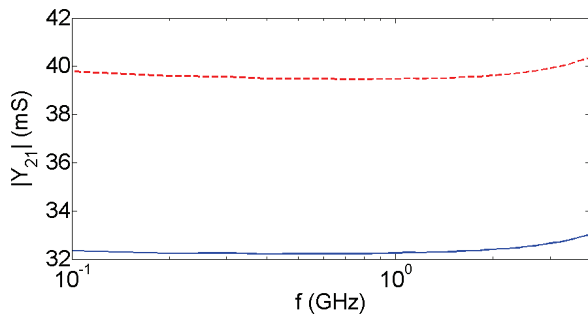

Fig. 6. Magnitude of Y_{21} versus frequency without light (blue continuous line) and under optical illumination at 650 nm (red dashed line) for a 100-µm HEMT at V_{GS} = -0.6 V and V_{DS} = 2.5 V. The frequency ranges goes from 0.1 to 4 GHz

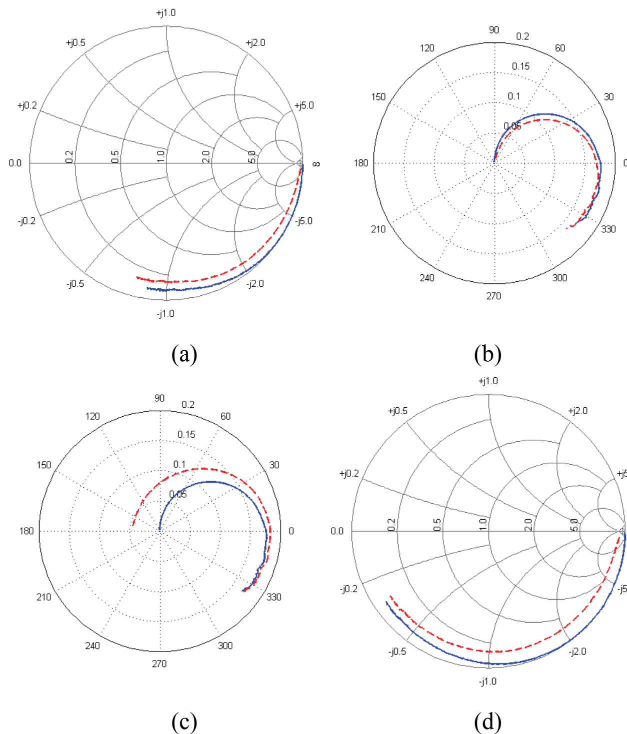

Fig. 7. S-parameters without light (blue continuous lines) and under optical illumination at 650 nm (red dashed line) for a 100-µm HEMT at V_{GS} = -1.275 V and V_{DS} = 0 V: (a) S_{11}, (b) S_{12}, (c) S_{21}, (d) S_{22}. The frequency ranges goes from 0.1 to 26.5 GHz

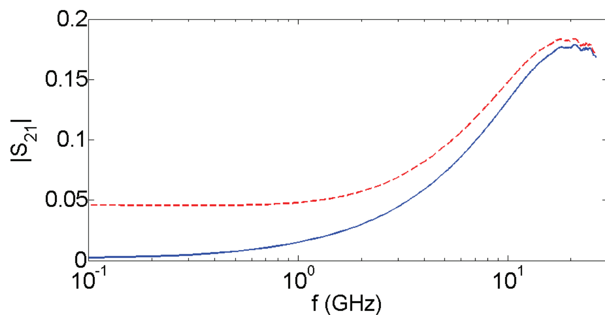

Fig. 8. Magnitude of S_{21} versus frequency without light (blue continuous line) and under optical illumination at 650 nm (red dashed line) for a 100-µm HEMT at V_{GS} = -1.275 V and V_{DS} = 0 V. The frequency ranges goes from 0.1 to 26.5 GHz

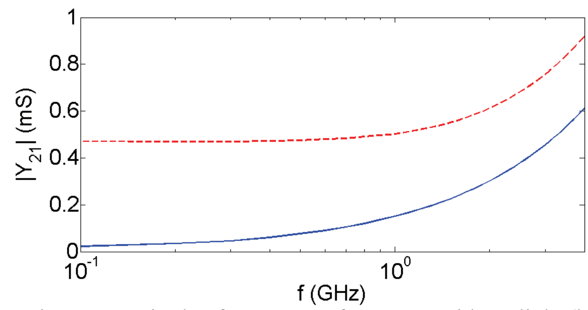

Fig. 9. Magnitude of Y_{21} versus frequency without light (blue continuous line) and under optical illumination at 650 nm (red dashed line) for a 100-µm HEMT at V_{GS} = -1.275 V and V_{DS} = 0 V. The frequency ranges goes from 0.1 to 4 GHz

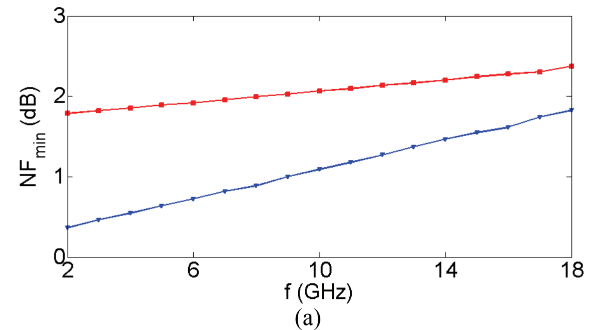

(a)

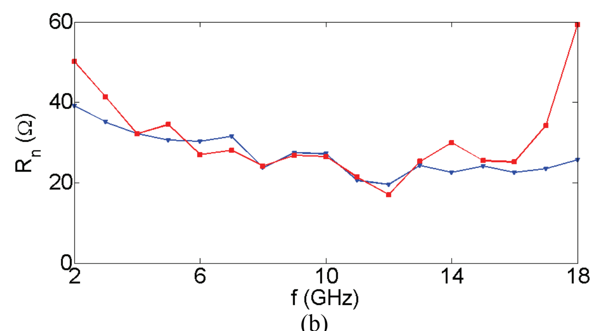

(b)

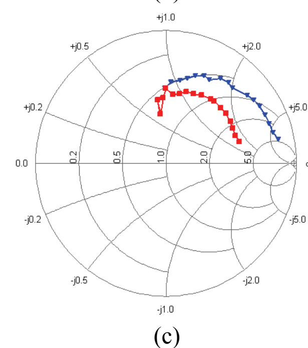

(c)

Fig. 10. N-parameters without light (blue lines) and under optical illumination at 650 nm (red line) for a 100-µm HEMT at V_{GS} = -0.6 V and V_{DS} = 2.5 V: (a) NF_{min}, (b) R_n, (c) Γ_{opt}. The frequency ranges goes from 2 to 18 GHz

Finally, to highlight the impact of the light exposure on the noise behaviour, Fig. 11 shows the elliptic paraboloid obtained by the 3D representation of the noise figure as a function of the source reflection coefficient. To illustrate the frequency dependence of the optical effects for the noise paraboloid, the data with and without optical illumination have been reported for three different frequencies: 2 GHz, 10 GHz, and 18 GHz.

VI. Conclusions

An extensive experimental study of the DC and microwave behaviour of AlGaAs/GaAs HEMTs under optical illumination has been presented. Three different devices with a gate width of 100 µm, 200 µm, and 300 µm have been studied. Three different laser wavelengths have been used, namely 960 nm, 808 nm, and 650 nm. The light sensitivity has resulted to be more pronounced in the smallest device and at shorter wavelength. Our experimental results have shown that the light exposure leads to a remarkable increase of the drain current and the transconductance. This could be ascribed to the threshold voltage shift arising from the internal photovoltaic effect. As a consequence, the analysis of the scattering parameters has shown that also the device gain is significantly improved under optical illumination. On the other hand, the study of the noise parameters has highlighted that the minimum noise figure is degraded under illumination because of the onset of high diffusion noise processes in the channel, which plays a more dominant role than the increase of the device gain.

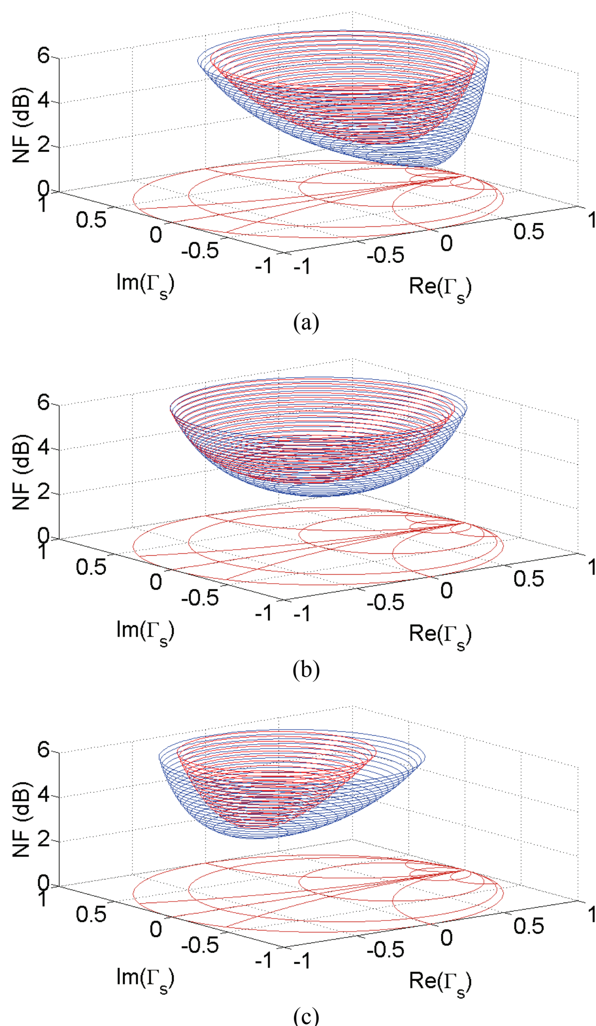

Fig. 11. Noise paraboloid representing the noise figure as a function of the source reflection coefficient without light (blue) and under optical illumination at 650 nm (red) for a 100-µm HEMT at V_{GS} = -0.6 V and V_{DS} = 2.5 V. The different frequencies goes have been analysed: (a) 2 GHz, (b) 10 GHz, and (c) 18 GHz

Acknowledgement

This is an extended version of the paper "Analysis of Microwave Noise Parameters of Scaled AlGaAs/GaAs HEMT's under Light Exposure" presented at the 11th International Conference on Telecommunications in Modern Satellite, Cable and Broadcasting Services - TELSIKS 2013, held in October 2013 in Niš, Serbia.

This work was supported by the Italian Ministry of Education, University and Research (MIUR) under the project PON01_01322 PANREX.

References

[1] M.W. Pospieszalski, "Modeling of noise parameters of MESFET's and MODFET's and their frequency and temperature dependence," *IEEE Trans. Microw. Theory Tech.*, vol. 37, no. 9, pp. 1340-1350, Sept. 1989.
[2] A. Caddemi, G. Martines, and M. Sannino, "HEMT for low noise microwaves: CAD oriented modeling," *IEEE Trans. Microw. Theory Tech.*, vol. 40, no. 7, pp. 1441-1445, Jul. 1992.
[3] A. Caddemi, G. Martines, and M. Sannino, "Automatic characterization and modeling of microwave low-noise HEMT's," *IEEE Trans. Instrum. Meas.,* vol. 41, no. 6, pp. 946-950, Dec. 1992.
[4] G. Dambrine, H. Happy, F. Danneville, and A. Cappy, "A new method for on wafer noise measurement," *IEEE Trans. Microw. Theory Tech.*, vol. 41, no. 3, pp. 375-381, Mar. 1993.
[5] F. Giannini, E. Limiti, G. Orengo, and G. Saggio, "Broadband peaking techniques for HEMT-based monolithic transimpedance amplifiers", *Microw. Opt. Technol. Lett.*, vol. 24, no. 3, pp. 147-151, Feb. 2000.
[6] Z. Marinkovic and V. Markovic "Temperature-dependent models of low-noise microwave transistors based on neural networks," *Int. J. RF Microw. Comput.-Aided Eng.*, vol. 15, no. 6, pp. 567-577, Nov. 2005.
[7] Z. Marinkovic, O. Pronić, and V. Markovic "Artificial neural network applications in improved noise wave modeling of microwave FETs," *Microw. Opt. Technol. Lett.*, vol. 50, no. 10, pp. 2512-2516, Oct. 2008.
[8] A. Caddemi and G. Crupi, "On the noise measurement and modelling for on wafer HEMTs up to 26.5 GHz," *Microw. Opt. Technol. Lett.*, vol. 52, no. 8, pp. 1799-1803, Aug. 2010.
[9] M. W. Pospieszalski, "Interpreting transistor noise," *IEEE Microw. Mag.*, vol. 11, no. 6, pp. 61-69, Oct. 2010
[10] F. Danneville, "Microwave noise and FET devices," *IEEE Microw. Mag.*, vol. 11, no. 6, pp. 53-60, Oct. 2010.
[11] R. Simons, "Microwave performance of an optically controlled AlGaAs/GaAs high electron mobility transistor and GaAs MESFET," *IEEE Trans. Microw. Theory Tech.*, vol. 35, no. 12, pp. 1444-1455, Dec. 1987.
[12] A. De Salles and M. Romero, "$Al_{0.3}Ga_{0.7}As$/GaAs HEMT's under optical illumination," *IEEE Trans. Microw. Theory Tech.*, vol. 39, no. 12, pp. 2010-2017, Dec. 1991.
[13] H. Yajian and A. Alphones, "Frequency-dependent behavior of optically illuminated HEMT," *Microw. Opt. Technol. Lett.*, vol. 30, no. 2, pp. 138-142, Jul. 2001.
[14] M. Somerville, A. Ernst, and J. Del Alamo, "A physical model for the kink effect in InAlAs/InGaAs HEMT's," *IEEE Trans. Electron Dev.*, vol. 47, no. 5, pp. 922-930, May 2000.
[15] R. Vandersmissen, D. Schreurs, S. Vandenberghe, and G. Borghs, "Optical control of a backside illuminated thin-film metamorphic HEMT," *Gallium Arsenide Applications Symposium*, Milano, Italy, Sept. 2002.

[16] Y. Takanashi, K. Takahata, and Y. Muramoto, “Characteristics of InAlAs/InGaAs high-electron mobility transistors under 1.3-μm laser illumination,” *IEEE Electron Dev. Lett.*, vol. 19, no. 12, pp. 472-474, Dec. 1998.

[17] Y. Takanashi, K. Takahata, and Y. Muramoto, “Characteristics of InAlAs/InGaAs high-electron mobility transistors under illumination with modulated light,” *IEEE Trans. Electron Dev.*, vol. 46, no 12, pp. 2271-2277, Dec. 1999.

[18] R. Vandersmissen, D. M. M.-P. Schreurs, S. Vandenberghe, and G. Borghs, “A time- and frequency-domain characterization of a thin-film metamorphic HEMT under modulated backside illumination*,” Int. J. RF Microw. Comput.-Aided Eng.*, vol. 14, no. 6, pp 535-542, Nov. 2004.

[19] M. A. Romero, M. A. G. Martinez ,and P. R. Herczfeld, “The photoresponse of microwave HEMTs: Semi-analytical modeling,” *IEEE/SBMO MTT-S Microwave and Optoelectronics Conference*, Rio de Janeiro, Brazil, Jul. 1995, pp. 749-754.

[20] M. Romero, L. De Barros, and P. R. Herczfeld, “Internal photovoltaic effects in microwave devices,” *IEEE MTT-S International Microwave Symposium Digest*, San Diego, CA, USA, May 1994, pp. 1505-1508.

[21] L. Escotte, K. Grenier, J. G. Tartarin, and J. Graffeuil, “Microwave noise parameters of InGaAs pseudomorphic HEMTs under optical illumination,” *IEEE Trans. Microw. Theory Tech.*, vol. 46, no. 11, pp. 1788-1789, Nov. 1998.

[22] A. Thomasian, A. Rezazadeh, J. Everard, and I. Ipwood, “Experimental evidence for trap-induced photoconductive kink in AlGaAs/GaAs HEMT’s,” *Electron. Lett.*, vol. 26, no. 14, pp. 1094-1095, Jul. 1990.

[23] A. Caddemi, G. Crupi, E. Fazio, S. Patanè, and G. Salvo, “Analysis of microwave noise parameters of scaled AlGaAs/GaAs HEMT’s under light exposure,” *IEEE International Conference on Telecommunications in Modern Satellite, Cable and Broadcasting Service (TELSIKS)*, Nis, Serbia, 16-19 October 2013, pp. 178-183.

[24] A. Caddemi, G. Crupi, E. Fazio, S. Patanè, and G. Salvo, “Remarks of an extensive investigation on the microwave HEMT behavior under illumination,” *IEEE Microw. Wireless Comp. Lett..*, vol. 24, no. 2, Feb. 2014.

[25] G. Crupi and D. M. M.-P. Schreurs, *Microwave De-embedding: From Theory To Applications*. Oxford, UK: *Academic Press*, 2014.

[26] J.-M. Collantes, R. D. Pollard, and M. Sayed, “Effects of DUT mismatch on the noise figure characterization: a comparative analysis of two Y-factor techniques,” *IEEE Trans. Instrum. Meas.*, vol. 51, no. 6, pp. 1150-1156, Dec. 2002.

[27] “Fundamentals of RF and Microwave Noise Figure Measurements,” Agilent Application Note 57-1, 2010.

[28] G. Crupi, A. Caddemi, D. M. M.-P. Schreurs, W. Wiatr, and A. Mercha, “Microwave noise modeling of FinFETs,” *Solid-State Electron.*, vol. 56, no 1, pp. 18-22, Feb. 2011.

[29] G. Crupi, D. M. M.-P. Schreurs, J.-P. Raskin, and A. Caddemi, “A comprehensive review on microwave FinFET modeling for progressing beyond the state of art,” *Solid-State Electron.*, vol. 80, pp. 81-95, Feb. 2013.

[30] D. Miller, D. Chemla, and S. Schmitt-Rink, “Relation between electroabsorption in bulk semiconductors and in quantum wells: The quantum confined Franz-Keldysh effect,” *Phys. Review B*, vol. 33, no. 10, pp. 6976-6982, May 1986.